Microparticle charging in dry air plasma created by an external ionization source

I N Derbenev and A V Filippov

State Research Center of the Russian Federation – Troitsk Institute for Innovation and Fusion Research, Pushkovykh Street 12, Troitsk, Moscow 142190, Russia

E-mail: derbenev@triniti.ru

Abstract. In the present paper the dust particle charging is studied in a dry air plasma created by an external ionization source. The ionization rate is changed in the range 10^1–10^{20} $\mathrm{cm}^{-3}\mathrm{s}^{-1}$. It is found that the main positive ion of the plasma is O_4^+ and the main negative ones are O_2^- and O_4^-. The point sink model based on the diffusion-drift approach shows that the screening potential distribution around a dust particle is a superposition of four Debye-like exponentials with four different spatial scales. The first scale almost coincides with the Debye radius. The second one is the distance, passed by positive and negative plasma components due to ambipolar diffusion in their recombination time. The third one is defined by the negative ion conversion and diffusion. The fourth scale is described by the electron attachment, recombination and diffusion at low gas ionization rates and by the recombination and diffusion of negative diatomic ions at high ionization rates. It is also shown that the electron flux defines the microparticle charge at high ionization rates, whereas the electron number density is much less than the ion one.

1. The main ions in dry air plasma

The ion components of the plasma are obtained by the analysis of ion-molecular reactions from [1] and the processes caused by an electron beam:

$$\mathrm{O_2} + \mathrm{e}_b \to \mathrm{O_2^+} + \mathrm{e} + \mathrm{e}_b, \quad \mathrm{O_2} + \mathrm{e}_b \to \mathrm{O^+} + \mathrm{O} + \mathrm{e} + \mathrm{e}_b,$$
$$\mathrm{N_2} + \mathrm{e}_b \to \mathrm{N_2^+} + \mathrm{e} + \mathrm{e}_b, \quad \mathrm{N_2} + \mathrm{e}_b \to \mathrm{N^+} + \mathrm{N} + \mathrm{e} + \mathrm{e}_b.$$

The resulting densities are presented in table 1. Calculations reveal that the main positive ion type is O_4^+ and the main negative ion types are O_2^- and O_4^-.

2. The microparticle charging in plasma of an electronegative gas

The microparticle charging is described by the hydrodynamic equation system:

$$\begin{aligned}
&\frac{\partial n_e}{\partial t} + \mathrm{div}\mathbf{j}_e = Q_{\mathrm{ion}} - \beta_{ei} n_e n_i - \alpha n_e,\\
&\frac{\partial n_i}{\partial t} + \mathrm{div}\mathbf{j}_i = Q_{\mathrm{ion}} - \beta_{ei} n_e n_i - \beta_{ii2} n_i n_2 - \beta_{ii4} n_i n_4,\\
&\frac{\partial n_2}{\partial t} + \mathrm{div}\mathbf{j}_2 = \alpha n_e - \nu_{24} n_2 + \nu_{42} n_4 - \beta_{ii2} n_i n_2,\\
&\frac{\partial n_4}{\partial t} + \mathrm{div}\mathbf{j}_4 = \nu_{24} n_2 - \nu_{42} n_4 - \beta_{ii4} n_i n_4,
\end{aligned} \tag{1}$$

Table 1. The steady-state electron and ion number densities at three different gas ionization rates.

Q_{ion}	10^{14} cm^{-3}s^{-1}	10^{16} cm^{-3}s^{-1}	10^{18} cm^{-3}s^{-1}
n_e	2.077×10^6	2.058×10^8	1.929×10^{10}
O_2^-	1.856×10^{10}	1.841×10^{11}	1.720×10^{12}
O_4^-	1.054×10^{10}	1.045×10^{11}	9.735×10^{11}
O_4^+	2.515×10^{10}	2.506×10^{11}	2.401×10^{12}
$NO^+ \cdot O_2$	2.707×10^9	2.564×10^{10}	1.727×10^{11}
NO_2^+	1.132×10^9	1.140×10^{10}	1.212×10^{11}
O_2^+	1.138×10^8	1.168×10^9	1.451×10^{10}
$O_2^+ \cdot N_2$	3.055×10^6	3.135×10^7	3.888×10^8
NO^+	2.446×10^5	2.316×10^7	1.577×10^9
$NO^+ \cdot N_2$	5.464×10^4	5.175×10^6	3.521×10^8
N_4^+	4.952×10^4	4.451×10^6	4.948×10^8
N_3^+	3.406×10^4	3.406×10^6	3.400×10^8
N_2^+	3.095×10^3	3.095×10^5	3.094×10^7
N^+	8.356×10^2	8.355×10^4	8.347×10^6
O^+	2.287×10^2	2.287×10^4	2.286×10^6

supplemented by the Poisson equation:

$$\Delta\phi = -4\pi e \left(n_i - n_2 - n_4 - n_e\right). \tag{2}$$

Here $\mathbf{j}_e = -\text{sign}\left(e_\sigma\right)\mu_\sigma n_\sigma \nabla\phi - D_\sigma \nabla n_\sigma$ are the fluxes of the corresponding particle type ($\sigma = e$, i, 2, 4); e_σ is the charge of the σ-particle, e is the elementary charge ($e_i = e$, $e_e = e_2 = e_4 = -e$); n_σ is the number density of electrons ($\sigma = e$), of positive ions O_4^+ ($\sigma = i$), of negative ions O_2^- and O_4^-; μ_σ and D_σ are the mobility and diffusion coefficients respectively; β_{ei} is the recombination coefficient of electrons and ions O_4^+; β_{ii2} and β_{ii4} are the recombination coefficients of ions O_4^+ with O_2^- and O_4^- respectively; α is the attachment coefficient; ν_{24} and ν_{42} are the coefficients of conversion of the two-atom ions into the four-atom ones and vice versa.

The system of equations (1) and (2) is solved by linearization and three-dimensional Fourier transform. The screening potential around a charged particle is found to be a superposition of four exponentials:

$$\phi\left(r\right) = \frac{eq}{r}\sum_{j=1}^{4} C_j \exp\left(-k_{shj} r\right). \tag{3}$$

Calculations reveal that complex constants appear in the limited region of Q_{ion} values. In this case the potential takes the form:

$$\phi\left(r\right) = \frac{eq}{r}\Big\{C_1 \exp\left(-k_{sh1} r\right) + C_2 \exp\left(-k_{sh2} r\right) + \exp\left(-\kappa_3 r\right)\left[Q_3 \cos\left(\kappa_4 r\right) + Q_4 \sin\left(\kappa_4 r\right)\right]\Big\}, \tag{4}$$

where $\kappa_3 = \frac{1}{2}\left(k_{sh3} + k_{sh4}\right)$, $\kappa_4 = \frac{i}{2}\left(k_{sh4} - k_{sh3}\right)$, $Q_3 = \frac{1}{2}\left(C_3 + C_4\right)$, $Q_4 = \frac{i}{2}\left(C_4 - C_3\right)$.

3. The comparison of the numerical and analytical calculations

The physical meaning of the screening constants is established within the analytical solution of particular cases of the system of equations (1) and (2). It is revealed, that the first constant is

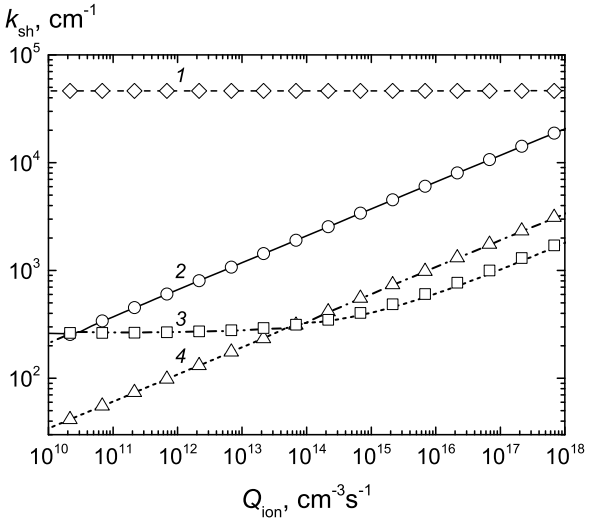

Figure 1. The comparison of the numerical and analytical calculation of the screening constants. The real parts of the screening constants are found by numerical calculations: *1* – k_{sh1}, *2* – k_{sh2}, *3* – k_{sh3}, *4* – k_{sh4}; symbols represent their approximate values: ○ – k_D, △ – k_s, ◇ – k_{con}, □ – k_{e2}.

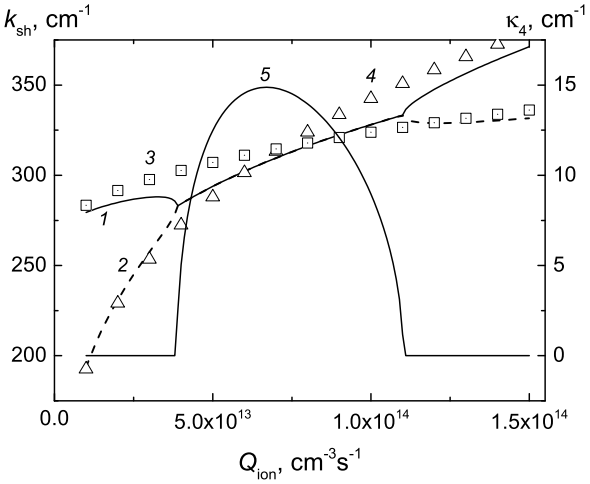

Figure 2. The dependance of screening constants on Q_{ion} in the crossing region of 3rd and 4th constants. *1* – k_{sh3}, *2* – k_{sh4}, *3* – k_s, *4* – k_{e2}, *5* – imaginary part of the screening constants κ_4.

the inverse Debye length:

$$k_D^2 = k_{De}^2 + k_{Di}^2 + k_{D2}^2 + k_{D4}^2,$$

where $k_{D\sigma}^2 = 4\pi e^2 n_{\sigma 0}/T_\sigma$ and $n_{\sigma 0}$ is the undisturbed number density of plasma components. The second one is the inverse length passed by positive and negative ions and electrons due to ambipolar diffusion in the characteristic recombination time:

$$k_s^2 \approx \beta_{ei} n_{e0} \left(D_i^{-1} + D_e^{-1}\right) + \beta_{ii2} n_{20} \left(D_i^{-1} + D_2^{-1}\right) + \beta_{ii4} n_{40} \left(D_i^{-1} + D_4^{-1}\right).$$

The third one is the inverse diffusion length of negative ions in their conversion time into each other:

$$k_{con} \approx \nu_{24} D_2^{-1} + \nu_{42} D_4^{-1}.$$

The fourth constant is defined by the electron attachment and recombination of electrons and diatomic oxygen ions:

$$k_{e2}^2 \approx (\alpha + \beta_{ei} n_{i0}) D_e^{-1} + \beta_{ii2} n_{20} D_2^{-1}.$$

The comparison of the numerical and analytical results of the screening constants is shown in figure 1.

Figure 1 shows the curve crossing in two regions of gas ionization rate: (1.8–3.4) $\times 10^{10}$ and (0.4–1.1) $\times 10^{14}$ cm^{-3}s^{-1}. It means that two of four screening constants have coincident real parts. This coincidence yields the complex constants. The imaginary part κ_4 of constants k_{sh3} and k_{sh4} is shown in figure 2 as the function of the air ionization rate.

According to the work [2] the electron and ion fluxes are approximately expressed in terms of their undisturbed number densities $n_{\sigma 0}$ far from microparticle as follows:

$$J_{\sigma 0} = -\frac{\beta_{L\sigma} n_{\sigma 0} z_\sigma q}{1 - \exp\left(z_\sigma e^2 q / T_\sigma r_0\right)}, \tag{5}$$

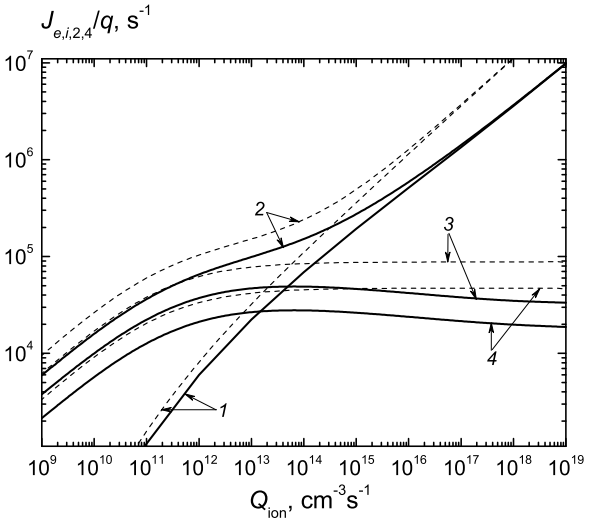

Figure 3. The plasma component fluxes on a microparticle versus air ionization rate $Q_{\rm ion}$: *1* – electrons, *2* – positive ions O_4^+, *3* and *4* – negative ions O_2^- and O_4^-, respectively. Solid curves are numerical calculations, dotted ones are analytical estimations (5).

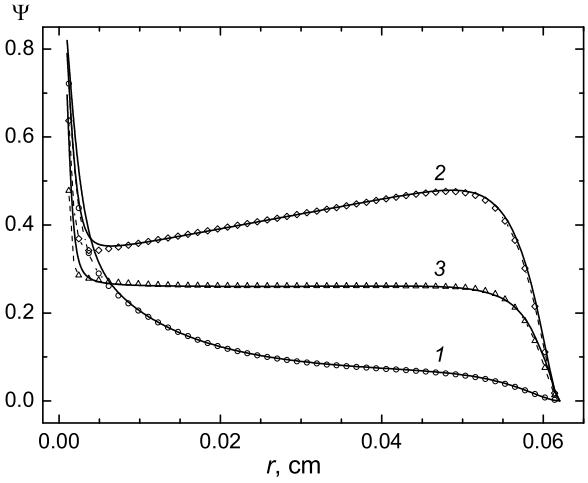

Figure 4. The reduced potential distribution $\Psi = \phi(r)/eq \times r(1+k_{sh4}r_0)\,e^{k_{sh4}(r-r_0)}$ around a dust particle at $Q_{\rm ion} = 10^{13}$ cm^{-3}s^{-1} (curve *1*), 10^{14} cm^{-3}s^{-1} (curve *2*) and 10^{15} cm^{-3}s^{-1} (curve *3*). The solid lines correspond to the numerical calculations, the dotted ones with symbols correspond to the sum of (7) with k_{sh4} and the Debye exponentials with k_{sh2} and k_{sh3} (for *1* and *3*), and the sum of (8), (9) and the Debye exponential with k_{sh2} (for *2*).

where $\beta_{L\sigma} = 4\pi e\mu_\sigma$ is the coefficient of Langevin recombination of σ-type particles on slow dust particles with charge $q = -z_\sigma$; $z_\sigma = 1$ for positive ions $\sigma = i$ and $z_\sigma = -1$ for $\sigma = e, 2, 4$. The comparison of analytical estimation (5) with numerical calculations is shown in figure 3.

Figure 3 shows that the equation (5) gives underestimated values due to assumption of flux uniformity that is not valid because of attachment, recombination and conversion processes. Nevertheless equation (5) gives proper qualitative character of dependencies. Although the electron number density is much less than the number density of oxygen negative ions (see table 1), the electron flux dominates in microparticle charging at gas ionization rates higher than 10^{14} cm^{-3}s^{-1} due to high electron mobility.

4. The potential distribution around microparticle

For the verification of the asymptotic theory equations (1) and (2) are solved numerically using finite-difference method with the following boundary conditions:

$$\begin{aligned} &n_\sigma|_{r=r_0} = 0; \quad n_\sigma|_{r=a_d} = n_{\sigma 0}; \\ &E|_{r=r_0} = \frac{q}{r_0^2}; \quad E|_{r=a_d} = 0; \quad \phi|_{r=a_d} = 0. \end{aligned} \tag{6}$$

Here n_d is the dust particle number density, $a_d = (4\pi n_d/3)^{-1/3}$ is the Wigner–Seitz cell radius. The solution of the equation (2) in a finite cell with boundary conditions (6) takes the form [3]:

$$\frac{q}{r}\left[B_1 \exp\left(-k_{sh4}r\right) + B_2 \exp\left(k_{sh4}r\right)\right] + B_3 \tag{7}$$

in case of real screening constants and

$$\frac{q}{r}\left[G_1 \exp\left(-\kappa_3 r\right) + G_2 \exp\left(\kappa_3 r\right)\right] \cos\left(\kappa_4 r\right) + G_3, \tag{8}$$

$$\frac{q}{r}\left[K_1 \exp\left(-\kappa_3 r\right) + K_2 \exp\left(\kappa_3 r\right)\right] \sin\left(\kappa_4 r\right) + K_3, \tag{9}$$

in case of complex ones. The coefficients B_i, G_i, K_i (i = 1–3) are found from the boundary conditions for the potential and the electric field strength (6).

The comparison of the potential analytical and numerical calculations at three different air ionization rates is shown in figure 4. This figure reveals that the expressions (7)–(9) are in good agreement with the numerical calculations. Note that numerical calculations identify properly only two smallest constants k_{sh3} and k_{sh4}, and the accuracy of the third-smallest constant k_{sh2} definition is rather low although this constant becomes apparent at short distances (the potential growth at $r < 0.01$ cm), where strong nonlinearity takes place as well as in the k_{sh1} appearance region. Thus the values of k_{sh1} and k_{sh2} obtained within the linear theory are almost physically meaningless.

Acknowledgments
This work was supported by the State Atomic Energy Corporation "ROSATOM" (state contract No. N.4h.44.90.13.1107), the Russian Foundation for Basic Research (project No. 15-02-06873) and a grant from the President of the Russian Federation (No. NSh-493.2014.2).

References

[1] Kossii I A, Kostinsky A Yu, Matveyev A A and Silakov V P 1992 *Plasma Source Sci. Technol.* **1** 207
[2] Fuchs N A 1963 *Geofisica Pura e Applicata* **56** 185
[3] Alexander S, Chaikin P M, Grant P, Morales G J, Pincus P and Honeet D 1984 *The Journal of Chemical Physics* **80** 5776